Investigation of the Pore Structure and Morphology of Cellulose Acetate Membranes Using Small-Angle Neutron Scattering. 1. Cellulose Acetate Active Layer Membranes

Sandeep Kulkarni[†] and Sonja Krause*

Polymer Science and Engineering Program & Department of Chemistry, Rensselaer Polytechnic Institute, Troy, New York 12180

G. D. Wignall

Solid State Division, Oak Ridge National Laboratory, Oak Ridge, Tennessee 37831

B. Hammouda

Center for High Resolution Neutron Scattering, National Institute of Standards and Technology, Gaithersburg, Maryland 20899

Received February 22, 1994[⊗]

ABSTRACT: The structure of ultrathin cellulose acetate membranes, known as active layer membranes, has been investigated using small-angle neutron scattering. These membranes are known to have structural and functional similarity to the surface or "skin" layer in commercial reverse-osmosis (RO) membranes and hence are useful model systems for understanding the structure of the RO membrane skin layer. Active layer membranes were studied after swelling them with either D_2O or CD_3OD. The results in both cases clearly indicated the presence of very small (10–20 Å) porous structures in the membrane. The presence of such pores has been a subject of long-standing controversy in this area. The data was analyzed using a modified Debye–Bueche analysis and the resultant membrane structure was seen to agree well with structural information from electron microscopic studies. Finally, a possible explanation for the differences in scattering observed between the D_2O swollen membranes and the CD_3OD swollen membranes has been presented.

Introduction

Over the last several decades synthetic polymeric membranes have found a wide range of applications in areas such as desalination, food processing, medicine, and pharmaceuticals. A large number of commercial membranes belong to two classes, namely, reverse–osmosis (RO) and ultrafiltration (UF) membranes. RO membranes are very highly selective and can prevent the passage of particles as small as a few angstroms in diameter, which accounts for the use of these membranes in desalination (involving removal of salt ions from aqueous solutions). UF membranes are less selective and can retain only particles larger than a few hundred angstroms in diameter and are hence used for filtration of macromolecules such as proteins from solutions.

Both RO and UF membranes are in general asymmetric in nature, that is, they consist of a thin, relatively dense film (usually referred to as the skin layer) supported by a porous sublayer. The skin layer is primarily responsible for selectively retaining certain materials and allowing the passage of others, while the sublayer provides mechanical support and allows high flux of permeable substances.

The first practical RO membrane composed of cellulose acetate (CA) was developed by Loeb and Sourirajan[1] and subsequently a large number of asymmetric (RO and UF) membranes utilizing a variety of different polymers have been prepared. A disadvantage of such membranes is that it is impossible to optimize the properties of the skin and the base layer independently of each other since both are formed integrally in a single step. To overcome this limitation a new class of membranes, known as composite membranes, was developed where the skin layer and the substructure could be fabricated separately and could in fact be prepared from different polymers. The first (and the simplest) of such membranes was devised by Francis[2] and consisted of an ultrathin film of cellulose acetate (~1000 Å thick) placed on top of a thick and highly porous cellulose acetate membrane prepared separately. It was demonstrated by Francis, and later by Riley[3] as well, that the ultrathin CA film mimicked the separation properties of the skin layer in an asymmetric membrane, as judged by its salt rejection. This suggested that these films were similar in structure to the skin layer of RO membranes. Such films will be referred to as "active layer membranes" in the present study.

While the importance of the skin layer in governing the separation properties of a membrane has long been recognized, relatively few studies aimed at understanding the skin structure have been reported, particularly in the case of RO membranes. This has resulted in an ongoing debate regarding the structure of the skin layer in RO membranes. Sourirajan[4] has suggested that the skin layer contains extremely small pores, with radii in the range of 5–15 Å, which exist only in the wet state of the membrane. Other authors,[5] however, maintained that the skin layer is completely nonporous and dense much like an ordinary polymer film.

Electron microscopic (EM) techniques provide the most direct means of observing the structure of materials, and a number of EM studies, primarily using transmission electron microscopy (TEM), have been reported on RO membranes. Riley[6] first investigated the surface structure of cellulose acetate RO membranes by observing a replica of the surface of a freeze-dried membrane under a TEM and found no evidence for the presence of pores on the surface. Later, Schultz[7] also studied surface replicas of cellulose acetate RO membranes using higher resolution EM techniques. He observed the presence of spherical structures, roughly 188 Å in diameter, on the surface of

[†] Present address: Department of Polymer Science and Engineering, University of Massachusetts, Amherst, MA 01003.

[⊗] Abstract published in *Advance ACS Abstracts*, October 1, 1994.

0024-9297/94/2227-6777$04.50/0

such membranes and he suggested that the skin layer of RO membranes consists entirely of closely packed spheres, as shown in Figure 1, with the interstitial voids acting as functional pores, selectively allowing passage of certain materials while rejecting others (such spheres have been commonly termed "nodules", and this terminology will be used in the present paper as well). Schultz also studied replicas of ultrathin CA films, similar to those prepared by Francis,[2] and observed striking similarities between the surface of such films and the surfaces of RO membranes, confirming the proposed similarity in the structure of the two systems.

It was later demonstrated by Panar[8] that this nodular morphology can be observed in the structure of RO membranes prepared from other polymers as well. Recently, Kamide[9,10] has delineated four levels of structure in asymmetric membranes prepared by phase inversion: macromolecules (the individual polymer chain), nodules (formed by aggregation of macromolecule chains), nodular aggregates, and supernodular aggregates. Kesting[11] has suggested that these four "tiers" of structure may all be simultaneously present in an asymmetric membrane. For instance, the skin layer in RO membranes is probably composed entirely of nodules and nodular aggregates. The functional pores in this case would be primarily the interstitial spaces (3–20 Å) between close-packed nodules.[7] According to Kesting, the interstitial regions in such a structure are probably regions of low density, rather than physical voids, consisting of polymer chains traversing from one nodule to another. Kesting also hypothesized that formation of nodular structures may occur by a nucleation and growth mechanism. However, recently Pinnau[12] has argued that such structures are most likely formed by spinodal decomposition followed by breakup of the resulting structure.

A number of authors have supported this view of the structure of the skinlayer largely on the basis of EM studies. All the EM studies to date have been performed on dried or freeze-dried membranes where the membrane is not in its "natural" (wet) state. Therefore very little is known about the structure of membranes in their wet state. Small-angle scattering, which is one of the relatively few techniques that allow a direct study of wet or solvent swollen membranes, is used in the present work in an attempt to resolve the controversy regarding the structure of the skin layer in RO membranes.

Small-angle X-ray scattering (SAXS) and small-angle neutron scattering (SANS) are widely used to study structures in the size range 10–1000 Å. These techniques involve measuring the intensity, $I(\mathbf{Q})$, of the scattered radiation as a function of $\mathbf{Q}$, where "$\mathbf{Q}$" is termed the scattering vector or the momentum transfer vector and is defined as

$$\mathbf{Q} = (4\pi/\lambda)\sin(\theta/2)$$

where λ is the wavelength of the incident radiation and θ is the scattering angle. For the effective use of small-angle scattering it is necessary to have a large difference in scattering ability between the object being studied and its surroundings (this difference is termed "scattering contrast"). In the case of SAXS, this corresponds to a difference in *electron densities* between the object and its surroundings, which in turn is related to a difference in their bulk densities. For SANS, the contrast is based on a difference in *neutron scattering length densities* between the structure of interest and the surrounding medium. The scattering length is a complex mathematical quantity describing the neutron scattering ability of a material (the scattering length density will be represented by "ρ" in later discussions) and it varies in an irregular manner for different atoms. For instance, the scattering length for hydrogen is very different from that for deuterium, and hence these two nuclei have very different scattering lengths.

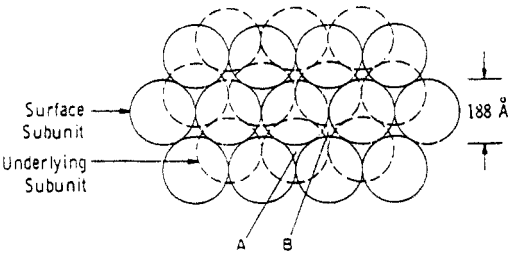

Figure 1. Structure of the skin layer of a cellulose acetate reverse-osmosis membrane idealized as an assembly of closely packed spheres.

In the present work, SAXS could not be used because, in the case of the wet membranes, the contrast between the swelling agent (water or methanol) in the pores and the membrane matrix polymer was insufficient to obtain a good scattering pattern. SANS, however, was the ideal technique since the membranes could be studied after swelling them with fully deuterated solvents (D_2O or CD_3OD) instead of the corresponding hydrogenous form of the solvents (H_2O or CH_3OH). The deuterated solvent in the pores thus provided a large contrast with the hydrogenous matrix polymer.

This paper will focus *only* on the structure of the active layer membranes (instead of a *complete* RO membrane consisting of the active layer *plus* a porous substructure) for the following reasons: (a) The information obtained on these membranes should lead to a better understanding of the skin layer in asymmetric RO membranes owing to their similarity in structure. (b) The results from the scattering experiments on active layer membranes should be easier to analyze since, in the case of a complete RO membrane, the thick porous base layer is expected to dominate the scattering pattern.

The scattering from *complete* RO and UF membranes and a comparison between the two systems is the subject of the following paper in this issue.[13]

Experimental Section

General. Cellulose acetate E 398-3 (Eastman Chemical Co.) was used in the preparation of the membranes described in this work. A sample of "pure" cellulose acetate (polymer free from additives and stabilizers) was kindly provided by C. M. Buchanan of Eastman Chemical Co. Reagent grade acetone (Mallinckrodt Chemicals), reagent grade formamide (Fisher Scientific), absolute ethanol (Aaper Alcohol and Chemical Co.), and hexane (Aldrich Chemical Co.) were used as received. Deuterium oxide (D_2O), 99.9 atom % D (MSD Isotopes), and deuterated methanol (CD_3OD), 99.8 atom % D (Cambridge Isotopes Laboratory), were used to swell the samples for neutron scattering studies. Distilled deionized water was used in all membrane casting procedures.

Sample Preparation. Ultrathin films were prepared by the vertical dipping procedure described by Riley.[3] A beaker containing a 2% solution of cellulose acetate in acetone was maintained at 30 ± 1 °C in a water bath. A clean glass plate was suspended, using a nylon thread above the solution, from the shaft of a 3 rpm reversible motor (a schematic of the arrangement is shown in Figure 2). The plate was slowly immersed in the solution, allowed to stand for 5 min, and then withdrawn slowly and raised slightly above the level of the solution. It was again allowed to stand for 20 min for evaporation of the solvent. The films so deposited on both surfaces of the glass plate were floated off on the surface of clean deionized water contained in a trough.[14] These films appeared highly uniform as judged by the lack of

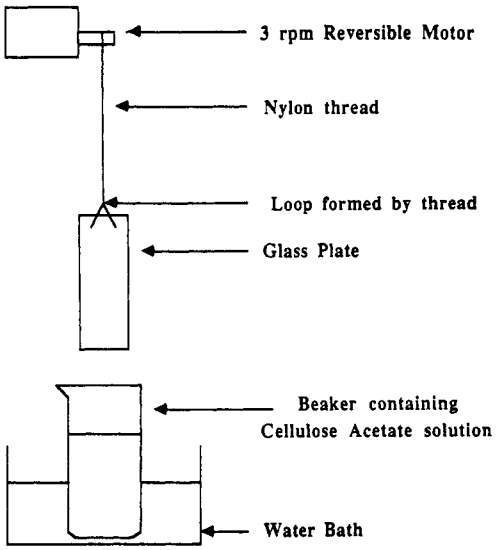

Figure 2. Schematic of the arrangement for the preparation of cellulose acetate ultrathin membranes.

interference coloration generally observed in nonuniform thin films. After floating off on water, these films were cut to an appropriate size. Individual films were deposited onto a suitable substrate by immersing the substrate into the water and "lifting off" the film from the surface. The film was allowed to dry in air after deposition. Multilayered samples were prepared by repeatedly retrieving films on the same substrate taking care to dry the substrate between two successive depositions. Samples consisting of approximately 1000 layers were prepared in this manner. Next this multilayered film was dried at ambient temperature in a vacuum oven for a period of 12 h. The sample at this stage was sufficiently thick to be handled as a free-standing film. The film was then detached from the substrate and folded over several times to obtain a 0.1–0.5 mm overall thickness for SANS studies.

Transmission Electron Microscopy (TEM). Cellulose acetate active layer films were prepared by the dipping technique described above. After floating the films off on the surface of water one of the films was deposited on a glass slide by immersing the slide below the film and then lifting it off from the surface of the water. After allowing the film to dry, the slide was placed in a Denton DV 502A vacuum evaporator, and the film was shadowed with Au–Pd alloy at an angle of ~9° (the low angle was used to enhance surface features).[7] Next, a thin (~200 Å) layer of carbon was deposited over the Au–Pd coating. The glass slide was then immersed in acetone for 1 h to dissolve the cellulose acetate and to release the replica from the slide. Pieces of the replica were retrieved onto copper grids and observed under a Philips CM 12 transmission electron microscope using an accelerating voltage of 80 kV. The resulting micrographs were digitized using an image scanner, and the gray scale was inverted using a computer. This inverted image simulates surface illumination of the membrane by light at a 9° angle.

Sample Cell for Small-Angle Neutron Scattering. A sketch of the sample cell used for all SANS experiments is shown in Figure 3. Multilayered samples of the active layer membranes were typically sandwiched between the two quartz windows using a Teflon gasket to maintain a small gap between the two windows. A brass ring and a top cover (with screw threads to allow it to be tightened against the ring) were used to retain the quartz windows in the cell. This gave an effective cell thickness of 1 mm. The lower part of the cell contained a small hole on one side, in line with the Teflon gasket. Samples were swollen inside the cell by inserting a syringe needle through this hole, piercing through the gasket and then injecting a small amount of the appropriate solvent into the gap containing the sample.

Small-Angle Neutron Scattering. SANS experiments were performed either at Oak Ridge National Laboratory (ORNL) or at the National Institute of Standards and Technology (NIST). The data at ORNL was obtained on a 30 m SANS instrument which has been described elsewhere.[15] Incident neutrons of wavelength 4.75 Å with a wavelength resolution ($\Delta\lambda/\lambda$) of 6% were used in all studies. The incident beam was collimated using source and sample slits separated by a distance of 10 m. An area detector with 64 × 64 cm^2 active elements (1 cm^2 element size) was positioned at two different distances, 10 and 1.5 m, from the sample to cover an effective $\mathbf{Q}$ range of 0.006–0.4 Å^{-1}. Scattering patterns were corrected for instrumental background and detector efficiency variation. The two-dimensional scattering patterns were circularly averaged and scattered intensity values converted to an absolute differential scattering cross section, $d\Sigma(\mathbf{Q})/d\Omega$ (determined for each value of $\mathbf{Q}$) per unit sample volume, using irradiated aluminum (Al-4) as a precalibrated secondary standard[16] (the units of the absolute cross section are cm^{-1}). Experiments at NIST were performed on a 30 m SANS instrument at the Center for High Resolution Neutron Scattering (CHRNS), which is a part of the Cold Neutron Research Facility (CNRF) at NIST. Neutrons of 5 Å wavelength with a spread ($\Delta\lambda/\lambda$) of 34% were used in these studies. A position sensitive detector, 65 × 65 cm^2 in area (with 1 cm^2 resolution), was used. Data were obtained at two different sample-to-detector distances, 13 and 3 m, to cover an effective $\mathbf{Q}$ range of 0.003–0.5 Å^{-1}. A retractable BF_3 detector was used to make transmission measurements. Scattering patterns were corrected and averaged as before. Conversion of scattered intensities to an absolute scale was carried out using two different calibration standards: a blend of deuterated/protonated polystyrene was used for calibration of low $\mathbf{Q}$ data while a 2 mm water sample was used to calibrate high $\mathbf{Q}$ data.

In all the above experiments, only the coherent scattering (where a fixed phase relationship exists between radiation scattered from different parts of a scattering object) from the membranes was of interest since this contains all the structural information about the membrane. Hence, in all cases the incoherent scattering (random phase relationship between scattered beams) was subtracted from the overall scattering pattern, before performing data analysis. The incoherent scattering was usually taken as the (constant) intensity where the scattering curves were seen to level off at high $\mathbf{Q}$, and the value for all samples was found to be approximately 0.25 cm^{-1}.

Scattering Theory Used in Data Interpretation. Scattering from random two-phase systems such as porous materials is frequently interpreted on the basis of the Debye–Bueche equation:[17]

$$\frac{d\sum(\mathbf{Q})}{d\Omega} = \frac{d\sum(0)}{d\Omega}\frac{1}{(1+\mathbf{Q}^2a^2)^2} \tag{1}$$

where $d\Sigma(\mathbf{Q})/d\Omega$ is the absolute differential cross section (proportional to the scattered intensity) and $d\Sigma(0)/d\Omega$ is its value at $\mathbf{Q} = 0$ ("zero angle" intensity). For simplicity of notation from this point on, $d\Sigma(\mathbf{Q})/d\Omega$ will be written simply as $I(\mathbf{Q})$ with the understanding that it represents the absolute cross section in units of cm^{-1}. The correlation length "a" describes fluctuations in scattering density in the material and is defined by the correlation function $\gamma(r)$:

$$\gamma(r) = \exp(-r/a) \tag{2}$$

For some systems the expression for the correlation function has been modified to include a Gaussian term:[18,19]

$$\gamma(r) = f\exp(-r/a_1) + (1-f)\exp(-r/a_2)^2 \tag{3}$$

where "f" is a fractional contribution for the two terms. The two correlation lengths in this expression, a_1 and a_2, are termed short-range and long-range correlation lengths, respectively. The scattered intensity (or the scattering cross section) in this case is given by

$$I(\mathbf{Q}) = (\rho_1-\rho_2)^2\phi(1-\phi)4\pi\left[\frac{2fa_1^3}{(1+\mathbf{Q}^2a_1^2)^2} + \frac{(1-f)\pi^{1/2}a_2^3}{4}\times \exp\left(-\frac{\mathbf{Q}^2a_2^2}{4}\right)\right] \tag{4}$$

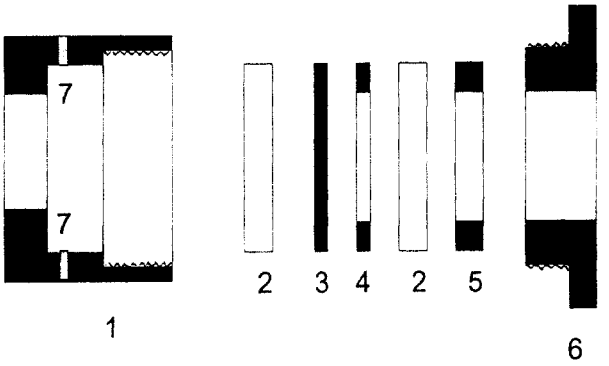

Figure 3. Sketch of sample cell used in SANS experiments: (1) brass sample cell (lower part), (2) quartz windows, (3) sample, (4) Teflon gasket, (5) brass O ring, (6) brass sample cell (upper part), (7) hole for injecting solvent.

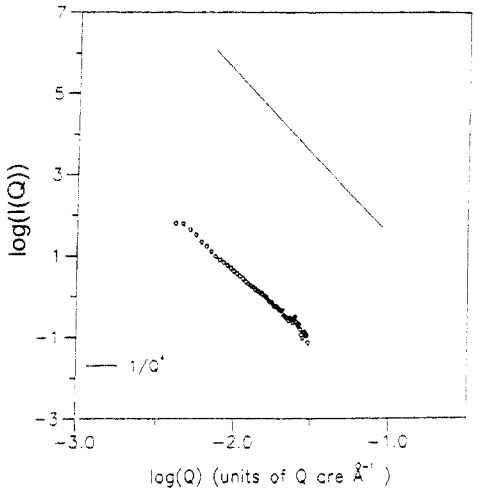

Figure 4. log I vs log **Q** plot for dry active layer membranes.

where ρ_1 and ρ_2 are the scattering length densities (as discussed previously) of the two phases and ϕ is the volume fraction of one phase.

For many systems the scattered intensity varies as $1/\mathbf{Q}^4$ at very large **Q** values, and this relationship is called Porod's law. In the case of the random two-phase systems discussed above, Porod's law behavior is expected if the interface between the two phases is assumed to be sharp.[20] In fact, it can be seen that the Debye–Bueche expression in eq 4 merges into the Porod's law scattering at high **Q** values (since the exponential term can be ignored and also the relation $\mathbf{Q}^2a_1^2 \gg 1$ holds at very high **Q**). In recent years fractal concepts have been used to describe the nature of pore surfaces for a number of porous materials, and it has been shown that such information can be obtained from small-angle scattering measurements. Bale[21] and Schmidt[22] have demonstrated that the scattering at high **Q** for a porous system, is given by the approximation

$$I(\mathbf{Q}) = A\mathbf{Q}^{-(6-D)} \tag{5}$$

where A is a constant and D is the so called "fractal dimension" which describes the roughness of the pore surfaces. The value of D varies from 2, for a smooth and uniform surface often termed "nonfractal", to 3 for a highly rough and irregular surface. It can be seen from eq 5 that, for a system which follows Porod's law ($I(\mathbf{Q}) \propto \mathbf{Q}^{-4}$), the fractal dimension must be 2, and this implies that the system contains smooth surfaces.

Results and Discussion

The scattering curve for a sample of dry active layer membrane is shown in Figure 4. The dry membrane was observed to be a relatively weak scatterer requiring long counting times to obtain good scattering patterns. Most of the scattered intensity in the plot appears at low **Q**

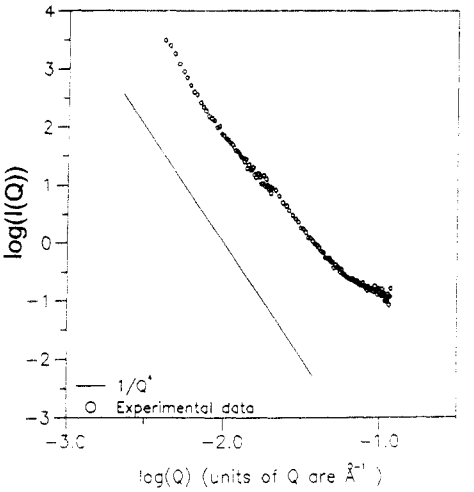

Figure 5. log I vs log **Q** plot for D_2O swollen active layer membranes.

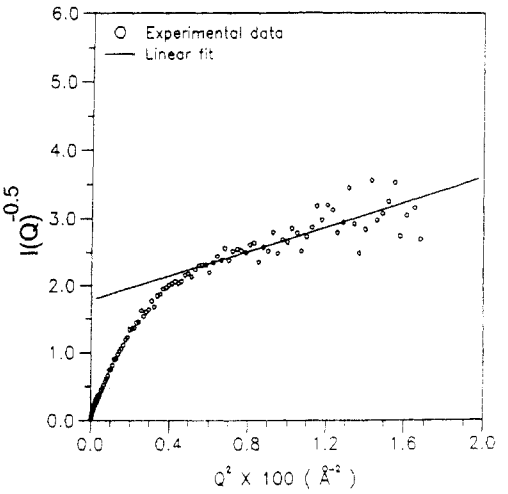

Figure 6. $I^{-0.5}$ vs $\mathbf{Q}^2$ (Debye–Bueche) plot for D_2O swollen active layer membranes.

values with almost no coherent scattering in the region $\mathbf{Q} > 0.4$ Å^{-1} (the scattering was observed to attain a constant value of $\sim$0.24 cm^{-1} in this region and this value was subtracted off as the incoherent scattering). Due to the weak scattering in the high **Q** region no conclusive arguments can be made regarding the presence or absence of pores, with radii less than $\sim$20 Å, in the dry membrane. However, the membrane does contain fairly large structures which scatter at low **Q**. The limited range of data available for this sample precluded any detailed analysis of its structure. It is worth mentioning that a SAXS scan obtained at NIST, for a similar dry sample, showed the same results, indicating that the same structure is probed by both techniques.

Figure 5 shows a log–log scattering curve of D_2O swollen active layer membranes. The straight lines in both Figures 4 and 5 represent the Porod's law ($\mathbf{Q}^{-4}$) relationship. The curve shows no evidence of a fourth power law behavior, at least in the **Q** region shown in Figure 5. The scattering at high **Q** indicates the presence of small pores in the swollen membrane (this data was obtained on the Oak Ridge instrument).

Figure 6 shows an $I^{-0.5}$ vs $\mathbf{Q}^2$ (Debye–Bueche) plot for the data shown in Figure 5. According to the expression in eq 4 involving two correlation lengths, the high **Q** region in a Debye–Bueche plot should be linear. The high **Q** data in this plot appears to be rather noisy. Nonetheless an *approximate* linear fit can be drawn, as shown in Figure

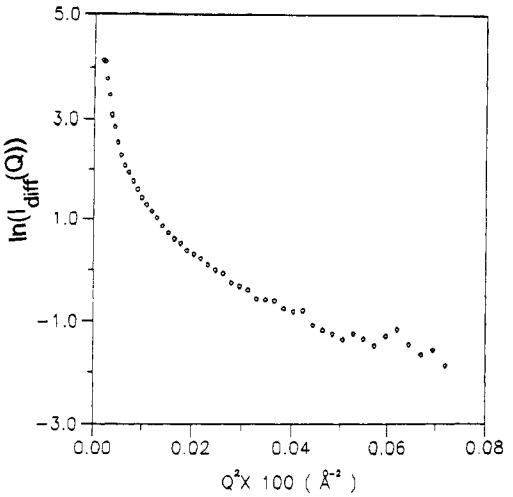

Figure 7. ln $I_{diff}(\mathbf{Q})$ vs $\mathbf{Q}^2$ plot for the low $\mathbf{Q}$ region of D_2O swollen active layer membranes.

6, and the slope of this fit gave a value of ~10 Å for the short-range correlation length, a_1. This value roughly corresponds to the radius of the interstitial pores predicted by Schultz[7] in his model (consisting of close packed nodules) for the RO membrane skin layer. Thus, the scattering data clearly demonstrates the presence of very small (<20 Å) solvent swollen porous regions in the membrane, thereby providing useful insight into the porous nature of these membranes.

It should be noted that the value of the correlation length indicates some *characteristic dimension* of the porous regions. This value can be converted into an equivalent pore radius by assuming some specific shape for the pores, such as spherical or cylindrical, but this has not been done in the present work for the following reasons: (a) It is *known* that the pores have irregular and tortuous shapes and it is highly unrealistic to approximate them as spheres or cylinders. (b) The values of pore radii quoted in the literature (obtained by permeation or microscopic techniques) themselves involve numerous approximations and cannot therefore be taken as exact.

Hence, in this and the following work[13] we compare only the *magnitude* of the correlation length to reported pore radii without concerning ourselves with the *exact values*. The correlation length will be referred to as the characteristic pore dimension rather than the pore radius (which is a difficult parameter to define for such systems in any case).

Next, the contribution due to the high $\mathbf{Q}$ term can be subtracted from the expression in eq 4, to obtain an I_{diff} which contains only the contribution due to the Gaussian correlation length (or the second term in eq 4). Hence, a plot of ln $I_{diff}(\mathbf{Q})$ vs $\mathbf{Q}^2$ should be a straight line whose slope contains the value of the long-range correlation length (a_2). As shown in Figure 7, such a plot is *not* a straight line and instead it appears to consist of a series of exponential slopes. In the present work, the model has therefore been modified to include multiple exponential terms (and hence multiple long-range correlation lengths) of the form

$$I_{diff} = A_2 \exp(-\mathbf{Q}^2 a_2^2/4) + A'_2 \exp(-\mathbf{Q}^2 a'^2_2/4) + \ldots \quad (6)$$

where a_2, a_2', etc., are the different values of the long-range correlation lengths which may correspond *either* to different *pore size distributions* or to the different *spacing* between pores.

Figure 8 shows a TEM micrograph of a surface replica of an active layer membrane, after computer digitization

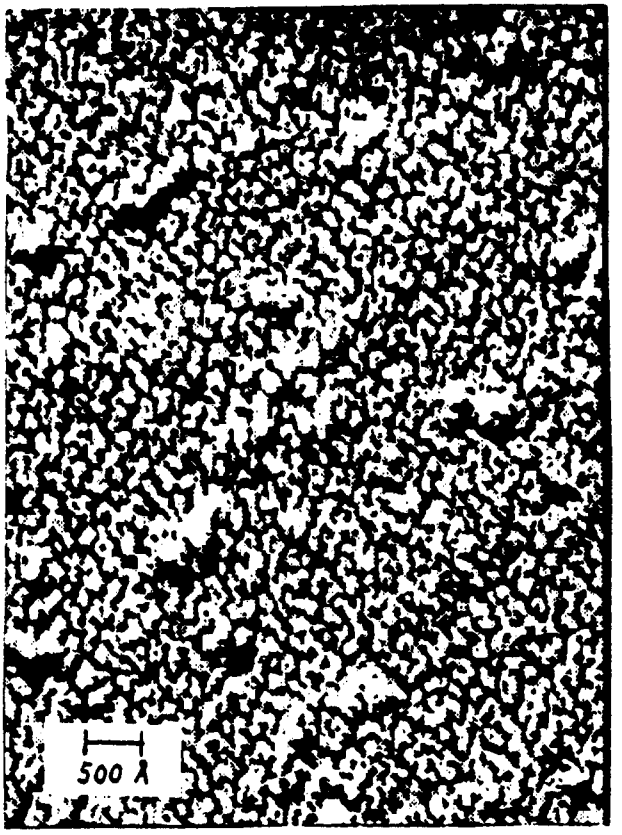

Figure 8. Transmission electron micrograph of a surface replica of an active layer membrane.

and inversion of the gray scale so that the white regions in the picture represent surface projections and the dark areas represent the shadow regions of such projections (as mentioned in the Experimental Section, this simulates an illumination of the surface at a low angle). The shadows are roughly circular with a relatively uniform diameter of about 200 Å, which corresponds to the size of nodules observed by various authors. There also appear to be few larger regions which may correspond to the larger nodular aggregates. Finally, the surface appears to be relatively "defect free"; i.e., no large (>100 Å) pores are present. Hence in the Debye–Bueche analysis involving multiple exponential terms, it would be reasonable to assume that the multiple values of the long-range correlation length, a_2, arise from *spacing between small pores* rather than from the presence of large pores.

A FORTRAN program called DISCRETE,[23,24] which fits multiexponential decays with up to five discrete exponential terms, was used to fit the low $\mathbf{Q}$ scattering data. A useful feature of this program is that it can determine the maximum number of exponential terms required (up to five) to best fit the data. This is provided as the best solution in the output, and other solutions containing fewer exponentials are also suggested (along with a plot of residuals for each solution). The program also provides the values of standard deviations for all the parameters determined by this analysis. In this work, the best solution (involving the maximum number of exponentials) was used in each case. For the D_2O swollen active layers, a reasonably good fit to the data was obtained using three exponentials (Figure 9) and the corresponding range of values for the long-range correlation length were a_2' = 550 Å, a_2'' = 200 Å, and a_2''' = 100 Å. The two larger values correspond (roughly) to the range of sizes expected for nodules and nodular aggregates, respectively. The smallest value of a_2 *might* reflect correlations between two adjacent D_2O-filled porous regions.

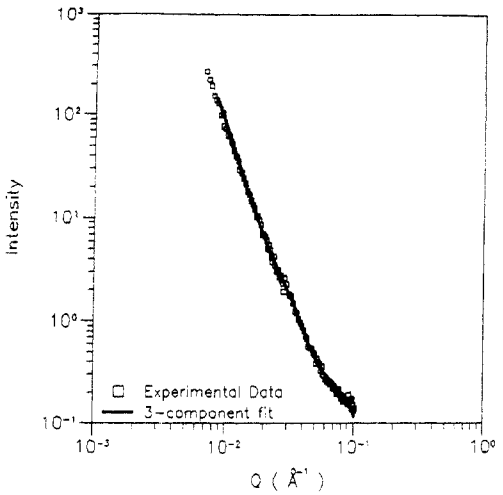

Figure 9. Scattering curve for a D_2O swollen active layer membrane with the three-exponential fit shown.

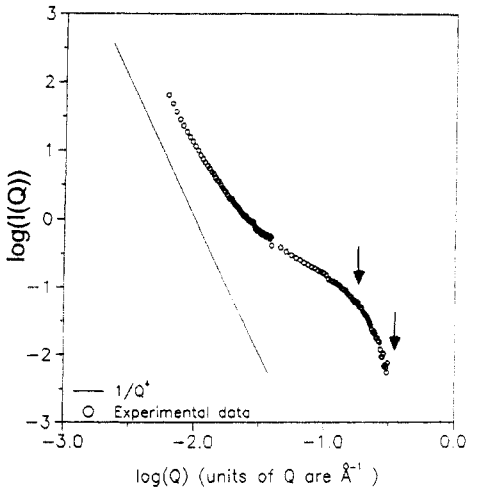

Figure 10. log $I(\mathbf{Q})$ vs log $\mathbf{Q}$ plot for a CD_3OD swollen active layer membrane. The arrows indicate the region where Porod's law behavior is observed.

It is well-recognized that, whenever more than two exponentials are needed to fit a set of data, these cannot give exact results and a different (larger) number of exponential terms could provide an equally good fit. Thus while the explanation based on the three correlation lengths is reasonable, a great deal of significance should not be attached to the values of the correlation lengths by themselves. These values are important only inasmuch as they indicate that the membrane contains structures with a *wide range of sizes* but they should not be taken to indicate the exact sizes.

These results are therefore in good agreement with the structure as seen under the TEM. As mentioned earlier, this structure has, until this time, been observed only in the dry or the freeze-dried state of the membrane. The present work represents the first direct study and corroboration of the structure of these membranes in the wet state.

A log–log scattering curve for a sample of the active layer membranes swollen with CD_3OD is shown in Figure 10. The scattering curve exhibits a marked change in slope at log $\mathbf{Q} \sim -0.7$ ($\mathbf{Q} \sim 0.2$ Å^{-1}) and appears to follow Porod's fourth power law at high $\mathbf{Q}$, as defined by the straight line in the plot. A power law behavior should *strictly* be observable over at least 1 order of magnitude of $\mathbf{Q}$ values; however, limitations of the instrument as well as beam time made it impractical to obtain data at higher $\mathbf{Q}$ values.

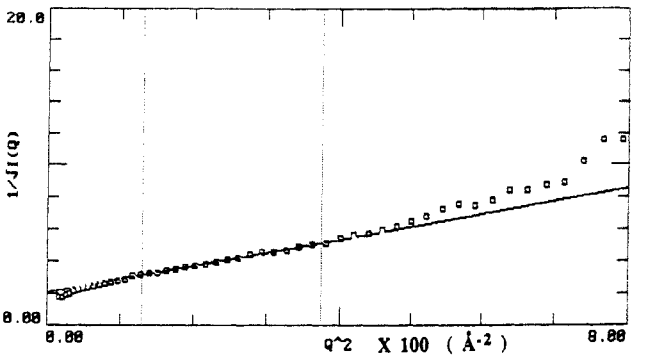

Figure 11. $(I(\mathbf{Q}))^{-0.5}$ vs $\mathbf{Q}^2$ plot for a CD_3OD swollen active layer membrane.

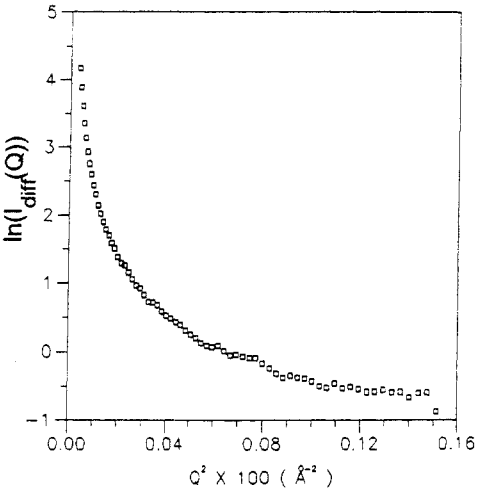

Figure 12. ln $I_{diff}(\mathbf{Q})$ vs $\mathbf{Q}^2$ plot for the low $\mathbf{Q}$ region of a CD_3OD swollen active layer membrane.

As discussed in the Theory section, the fourth power dependence indicates that the surface of the pores is smooth and nonfractal (fractal dimension of 2.0) and the pore–matrix interface is well-defined. This is an important result since little is known so far about the nature of the surface of the interstitial pores in such membranes.

The procedure for the data analysis in this case was exactly the same as that used for the D_2O swollen membrane. Figure 11 shows the $I^{-0.5}$ vs $\mathbf{Q}^2$ plot for the CD_3OD swollen sample. A linear fit to the relatively high $\mathbf{Q}$ region (the deviations from linearity observed at very high $\mathbf{Q}$ are due to the fourth power law dependence in this region which makes Debye–Bueche analysis inapplicable) gave a short-range correlation length: $a_1 \sim 10$ Å. Next, after subtraction of the high $\mathbf{Q}$ contribution, the remainder of the data (Figure 12) was fitted to a multiexponential expression. A good fit was obtained with two exponential terms and this gave the following values for the long-range correlation length: $a_2 = 400$ Å, $a_2' = 100$ Å.

Unlike the CD_3OD swollen samples the D_2O swollen membrane did not show a fourth power law in any region, as noted earlier. However the latter were studied only up to a maximum log $\mathbf{Q} \sim 0.01$ ($\mathbf{Q} \sim 0.125$ Å^{-1}) while the data for former extends to much higher $\mathbf{Q}$ values (this difference arises because the two sets of data were obtained on different instruments, the D_2O data at ORNL and the CD_3OD data at NIST). Figure 13 shows the D_2O and the CD_3OD data plotted on the same scale. The two curves appear to overlap at relatively high $\mathbf{Q}$ and in fact the D_2O curve *seems* to be approaching the limiting slope as well. Thus it is highly likely that the D_2O swollen membrane would exhibit the fourth power dependence if data at higher $\mathbf{Q}$ were to be obtained.

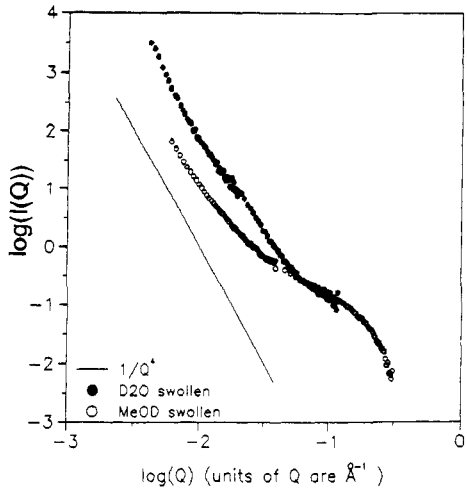

Figure 13. Scattering curves for D_2O and CD_3OD swollen active layer membranes plotted on the same (log–log) scale for comparison.

It can also be observed from Figure 13 that the two curves show significant differences at low **Q**. The higher scattering intensity in the case of the D_2O swollen sample cannot be explained solely on the basis of higher scattering contrast ($\Delta\rho$) between D_2O and cellulose acetate, as compared to the CD_3OD/cellulose acetate system, since a comparison of the contrast terms for the two cases[25] suggests that the scattering for D_2O swollen sample should be higher only by a factor of about 1.3. Therefore, the contrast factor cannot explain the large (roughly 1 order of magnitude) differences in scattered intensities at low **Q**.

These differences are most likely related to the different swelling "abilities" or effectiveness of D_2O and CD_3OD. On the basis of the previous results in the literature regarding the interaction of water with biological membranes, Schultz[7] stated that, for active layer membranes in their "natural" (wet) state, the water in the pores exists as an ordered cluster (called the hydration sheath) roughly 22 Å thick. The thickness and stability of such clusters is presumably a result of hydrogen bonding interactions between water and the hydrophilic polar groups on the surface of the pores. The ability of a solvent to hydrogen bond with cellulose acetate controls the thickness of the hydration sheath and hence the effective pore radius after swelling (since according to Schultz, the pore radius is roughly equal to the thickness of the hydration sheath). In the present study, D_2O is expected to have relatively strong hydrogen bonding interactions with cellulose acetate (almost equal to those in the case of ordinary water). Therefore the D_2O swollen membrane is expected to show a larger pore radius (as given by the short-range correlation length) than the CD_3OD swollen sample, since the CD_3OD forms relatively weaker hydrogen bonds with the polymer.

A change in pore radius upon swelling with different solvents should also result in a concomitant change in spacings between pores because as a result of swelling the nodules are pushed around to some extent thereby changing their spacing. This effect would be larger for the D_2O swollen sample, due to the higher degree of swelling, than for the CD_3OD swollen sample. Such an effect was indeed observed as reflected by the larger values of the long-range correlation lengths a_2, in the case of the D_2O swollen membrane. Finally it is worth noting that a relatively small change in the values of the long-range correlation lengths should result in a large change in the scattered intensity since a_2 appears as a power of an exponential term. This seems to explain rather well the differences observed between the low **Q** regions of the D_2O and CD_3OD swollen membranes.

Conclusions

In the present work, SANS was used to study active layer membranes in their dry state as well as after swelling them with D_2O or CD_3OD. On the basis of these experiments, the following conclusions can be drawn.

(1) The dry membrane showed no contribution from very small pores.

(2) Both the D_2O and the CD_3OD swollen membranes showed the presence of very small pores, and the average characteristic dimension of such pores was estimated as ~15 Å for the D_2O swollen sample and ~10 Å for the CD_3OD membrane. This is roughly comparable to the reported pore radii for such membranes.

(3) The values of the long-range correlation lengths obtained from the modified Debye–Bueche analysis compare favorably with the size of structures observed in electron micrographs of these membranes.

(4) The CD_3OD swollen membrane shows a fourth power law behavior at very high **Q** values, implying that the surface of the interstitial pores is smooth (non fractal) and well-defined.

(5) The differences in scattered intensity at low **Q** between the D_2O and the CD_3OD swollen membranes can be directly correlated with their respective ability for hydrogen bonding with cellulose acetate. This ability determines the effectiveness of a particular solvent to swell the membrane and hence it in turn determines the resultant pore size.

Acknowledgment. This research was supported in part by Grant CBT-8800649 from the National Science Foundation and in part by the Donors of the Petroleum Research Fund administered by the American Chemical Society. We wish to thank Dr. Takeshi Matsuura, National Research Council of Canada, for initiating us in the area of membrane preparation and for various valuable discussions. Work at Oak Ridge National Laboratory was supported by the US Department of Energy, under contract DE-AC05-840R-21400 with Martin Marietta Energy Systems Inc. SANS data at NIST were taken on the 30 m instrument supported by the National Science Foundation under agreement No. DMR-9122444. Identification of certain equipment or products does not imply recommendation by the National Institute of Standards and Technology. We thank Inga Green, Biology EM facility, Rensselaer Polytechnic Institute, for her assistance in the TEM experiments.

References and Notes

(1) Loeb, S.; Sourirajan, S. *UCLA Rep.* **1960**, 60–60.
(2) Francis, P.; Cadotte, J. *OSW R&D Prog. Rep.* **1964**, 177.
(3) Riley, R. L.; Lonsdale, H. K.; Lyons, C. R.; Merten, U. *J. Appl. Polym. Sci.* **1967**, *11*, 2143.
(4) Sourirajan, S. *Ind. Eng. Chem. Fund.* **1963**, *2*, 51.
(5) Lonsdale, H. K.; Merten, U.; Riley, R. L. *J. Appl. Polym. Sci.* **1965**, *9*, 1341.
(6) Riley, R. L.; Merten, U.; Gardner, J. O. *Desalination* **1966**, *1*, 30.
(7) Schultz, R. D.; Asunmaa, S. K. *Recent Prog. Surface Sci.* **1970**, *3*, 291.
(8) Panar, M.; Hoehn, H.; Herbert, R. *Macromolecules* **1973**, *6*, 777.
(9) Kamide, K.; Manabe, S. I. In *Materials Science of Synthetic Membranes*; Lloyd, D., Ed.; American Chemical Society Symposia Series; Washington, D.C., 1985; Vol. 269, pp 197–229.

(10) Kamide, K. *Thermodynamics of Polymer Solutions*, Elsevier: New York, 1990.
(11) Kesting, R. E. *J. Appl. Polym. Sci.* **1990**, *41*, 2739.
(12) Pinnau, I.; Koros, W. J. *J. Polym. Sci., Polym. Phys. Ed.* **1993**, *31*, 419.
(13) Kulkarni, S.; Krause, S.; Wignall, G. D. *Macromolecules*, following paper in this issue.
(14) Kulkarni, S. Ph.D. Thesis, Rensselaer Polytechnic Institute, Troy, New York, 1993.
(15) Koehler, W. C. *Physica (Utrecht)* **1986**, *137B*, 320.
(16) Wignall, G. D.; Bates, F. S. *J. Appl. Crystallogr.* **1987**, *20*, 28.
(17) Debye, P.; Bueche, A. M. *J. Appl. Phys.* **1949**, *20*, 518.
(18) Debye, P.; Anderson, H. R.; Brumberger, H. *J. Appl. Phys.* **1957**, *28*, 679.
(19) Moritani, M.; Inoue, T.; Motegi, M.; Kawai, H. *Macromolecules* **1970**, *33*, 433.
(20) Porod, G. In *Small Angle X-Ray Scattering*; Glatter, O., Kratky, O., Eds.; Academic Press: New York, 1982, pp 46–48.
(21) Bale, H. D.; Schmidt, P. W. *Phys. Rev. Lett.* **1984**, *53*, 596.
(22) Schmidt, P. W. In *Characterization of Porous Solids*; Unger, K. K., Ed.; Elsevier Science Publishers B.V.: Amsterdam, 1988; pp 35–48.
(23) Provencher, S. W. *J. Chem. Phys.* **1976**, *64*, 2722.
(24) Provencher, S. W. *Biophys. J.* **1976**, *16*, 27.
(25) The values for the scattering length densities for D_2O, CD_3OD, and cellulose acetate can be readily determined as described in ref 26 (the calculation for cellulose acetate was performed on the basis of one repeat unit, and this was assumed to have a density equal to the bulk density of cellulose acetate). From these values the value of the contrast, $\Delta\rho$, was obtained for the cellulase acetate/D_2O system as well as the cellulose acetate/CD_3OD system. Since the expression for the scattered intensity contains $(\Delta\rho)^2$, the relative contribution to the intensity due to the two solvents is given by

$$\frac{(\Delta\rho_{D_2O})^2}{(\Delta\rho_{CD_3OD})^2} \approx 1.3$$

(26) Stuhrmann, H. B. In *Small Angle X-Ray Scattering*; Glatter, O.; Kratky, O., Eds.; Academic Press: New York, 1982, pp 198–199.